$Sr_3Zr_2Cu_4Q_9$ (Q = S and Se): two novel layered quaternary mixed transition metal chalcogenides

Sayani Barman,[a] Sweta Yadav,[a] Akshay K. Ray,[a] Swati,[a] M. Deepa,[a] Manish K. Niranjan,[b] and Jai Prakash[a,*]

[a]*Department of Chemistry, Indian Institute of Technology Hyderabad, Kandi, Sangareddy, Telangana 502284, India*

[b]*Department of Physics, Indian Institute of Technology Hyderabad, Kandi, Sangareddy, Telangana 502284, India.*

*Corresponding author

E-mail address: jaiprakash@chy.iith.ac.in (Jai Prakash)

Electronic Supporting Information (ESI)

Section S1: Synthesizing single crystals and bulk $Sr_3Zr_2Cu_4Q_9$ (Q = S, Se)

The single crystals and bulk phases of the $Sr_3Zr_2Cu_4Q_9$ compounds were prepared using the high-temperature sealed-tube method. Various heating profiles were tried to synthesize single crystals and polycrystalline samples of the $Sr_3Zr_2Cu_4Q_9$ (Q = S, Se) to optimize the high-temperature reaction conditions. The optimized heating conditions for the reaction that produced single crystals of the $Sr_3Zr_2Cu_4Q_9$ (Q = S, Se) are the following. The reactants were first heated in a furnace from room temperature (RT) to 523 K in 6 h. Then, the temperature was maintained at 523 K for 12 h so that the molten sulfur/selenium could react with the metals. The exclusion of this step is expected to build high vapor pressure at high temperatures (>973 K) from chalcogens (S/Se) that can break the reaction tube. After heating the reactants at 523 K, the temperature of the furnace gradually increased to 1223 K in 18 h, and then the reaction mixture was dwelled for 12 h. Note that the complete phase diagram of the Sr-Zr-Cu-Q system is not known. Hence, the temperature of the furnace was increased gradually to avoid possible cracking of the tubes due to the excess vapor pressure of the chalcogens at high temperatures. Subsequently, the reaction mixture was cooled gradually to 1023 K in 67 h and then annealed at 1023 K for 96 h. The slow cooling step was used by assuming the growth of the crystals from liquid reactants at 1223 K. Afterward, the furnace's temperature was allowed to cool to 673 K in 72 h to improve the crystallinity of the product. Finally, the reaction mixture was allowed to cool radiatively to RT by shutting the furnace off.

The polycrystalline samples of the $Sr_3Zr_2Cu_4Q_9$ (Q = S, Se) were synthesized by heating the stoichiometric amounts of reactants inside vacuum-sealed fused silica tubes using the following heating profile. The sealed tubes containing the reaction mixtures were first heated

to 523 K over 3 h from RT, and then the furnace temperature was held constant for 10 h. After that, the reaction temperature was raised to 1223 K (in 36 h), and the reaction mixture was dwelled for 12 h. Following that, the reaction mixture was allowed to reach 1023 K in 12 h, and then annealing was done for four days. Lastly, the furnace slowly cooled to RT over 24 h.

A reddish-colored ingot was obtained from the high-temperature sealed tube reaction. The ingot was then crushed and homogenized into a fine powder inside the glove box. Next, a hydraulic press was used to compress the powder at about 15 MPa pressure into a circular pellet of 8 mm diameter. After that, the pellet was sealed in an evacuated fused silica tube, followed by heating it to 1023 K from RT for 12 h and sintering for 48 h. Finally, the tube was cooled down to RT in a period of 12 h. The final pellet was ground again, and the product was characterized using a powder X-ray diffraction study.

Section S2: CS_2 method to synthesize $Sr_3Zr_2Cu_4S_9$

We also tried to synthesize a polycrystalline $Sr_3Zr_2Cu_4S_9$ sample by heating the strontium carbonate ($SrCO_3$, 99.5%, SRL), zirconium dioxide (ZrO_2, 99.5%, SRL), and copper(I) oxide (Cu_2O, 99.7%, Alfa Aesar) under flowing CS_2 (99.5%, SDFCL) and N_2 gas admixture. The stoichiometric amounts of $SrCO_3$ and metal oxides of Zr and Cu were ball-milled using tungsten carbide bowls & balls to obtain a homogeneous reaction mixture that was pink in color.

$$3SrCO_3 + 2ZrO_2 + 2Cu_2O + nCS_2 \xrightarrow[N_2]{\Delta} Sr_3Zr_2Cu_4S_9 + nCO_2\uparrow$$

The reaction mixture of $SrCO_3$, ZrO_2, and Cu_2O in 1 g amount was transferred in an alumina boat and heated in a programmable tubular furnace under a flowing CS_2+N_2 gas mixture. The temperature profile of the CS_2 method is the following: firstly, the temperature was raised from RT to 1073 K over 3 h and the reactants were allowed to react for 9 h. Later, the reaction mixture was cooled to RT over 15 h. Once the reaction was done, the boat was taken out, the product was ground thoroughly, and the powder was characterized by the PXRD technique. The diffraction data showed the heating condition is preferable to form binary strontium sulfide as the major phase with additional unidentified amorphous phases rather than the pure desired quaternary compound. The setup details are described elsewhere.[1]

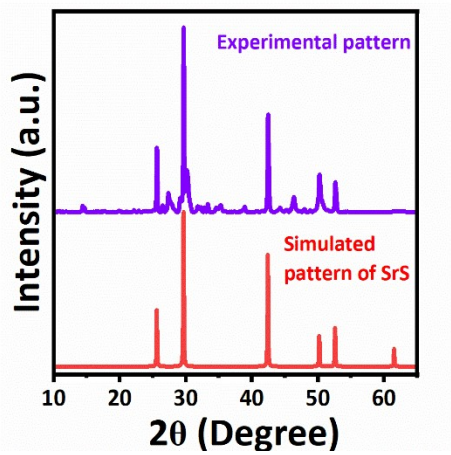

Fig. S1: The PXRD pattern of the reaction product (SrS, the major product) obtained from the sulfurization of the oxides and carbonates under the CS_2+ N_2 atmosphere.

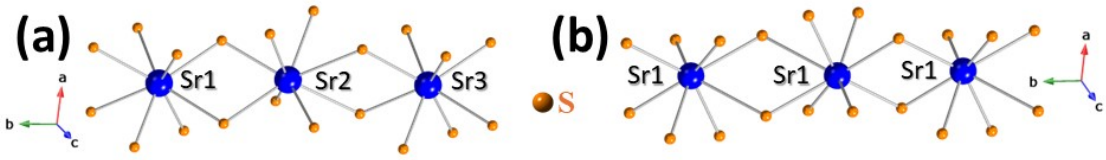

Fig. S2: The local coordination environments of **(a)** the Sr(1), Sr(2), and Sr(3) atoms in the $Sr_3Zr_2Cu_4S_9$ structure and **(b)** the Sr(1) atoms in the $Sr_3Zr_2Cu_4Se_9$ structure.

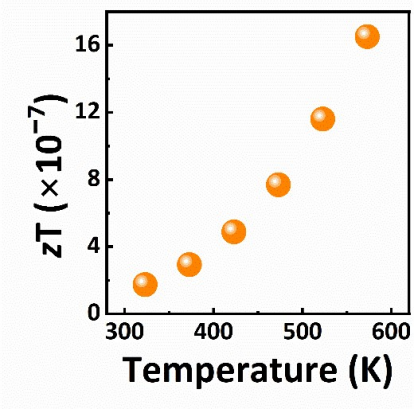

Fig. S3: The temperature-dependent zT plot of the $Sr_3Zr_2Cu_4Se_9$ sample. The Wiedemann-Franz Law,[2] which states that $\kappa_{ele} = LT/\rho$ (where L is the Lorenz number, T for absolute temperature, and ρ is electrical resistivity), was used to compute the electrical component of the total thermal conductivity or κ_{ele} values for the $Sr_3Zr_2Cu_4Se_9$ sample. The L value is dependent on the Seebeck coefficient (S) value, such as $L = 1.5 + \exp[-|S/116|]$. (where L is in 10^{-8} WΩ/K^2 and S in μV/K). For the aforementioned sample, the Seebeck or thermopower values are below ~25 μV/K; hence, according to the law, L values are found to be close to the degenerate limit of L (2.3×10^{-8} WΩ/K^2).

Section S3: Details of the computational studies of the $Sr_3Zr_2Cu_4Q_9$ structures

Density functional (DFT) calculations are performed on the $Sr_3Zr_2Cu_4Q_9$ structures.[3] The Coulomb potential of the nuclei and core electrons are approximated using the projected augmented wave (PAW) pseudopotentials.[4] A kinetic energy cutoff of 400 eV (or higher) sets the upper limit of the number of plane waves used in the basis. The $(4s^2,4p^6, 5s^2)$, $(4s^2,4p^6,4d^2, 5s^2)$, $(3d^{10}, 4s^1)$, $(3s^2, 3p^4)$, and $(4s^2,4p^4)$ electrons are treated as valence electrons in Sr, Zr, Cu, S, and Se atoms. The GGA-PBE scheme is used to approximate the exchange-correlation (XC) potential.[5] The improved estimates of bandgaps are also obtained using the GGA-1/2 scheme (See sec S4).[6] The reciprocal space integrations are performed by sampling the Brillouin zones using $(8 \times 5 \times 5)$ Monkhorst-Pack k-point meshes. The unit cells are optimized by reducing the Hellmann-Feynman atomic forces down to ~0.02 eV/Å (or less). The self-consistency in the calculations is achieved by converging the total energies down to 10^6 eV/cell. The optical absorption coefficient is estimated using the independent-particle approximation and from the electronic band structure.[7]

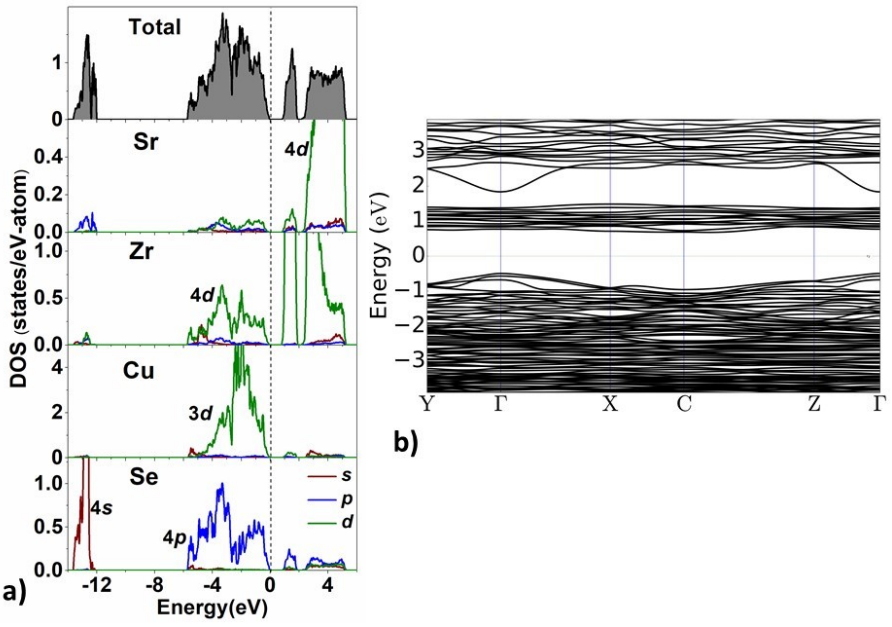

Fig. S4: (a) The total and projected density of states and the **(b)** band structure along high symmetry directions in the Brillouin zone for the $Sr_3Zr_2Cu_4Se_9$. The high symmetry k-points are $Y \equiv \left(0,\frac{1}{2},0\right)$, $\Gamma \equiv (0, 0, 0)$, $X \equiv \left(\frac{1}{2},0,0\right)$, $C \equiv \left(\frac{1}{2},\frac{1}{2},0\right)$, and $Z \equiv \left(0,0,\frac{1}{2}\right)$. The valence band maximum in (a) is indicated by the dotted line.

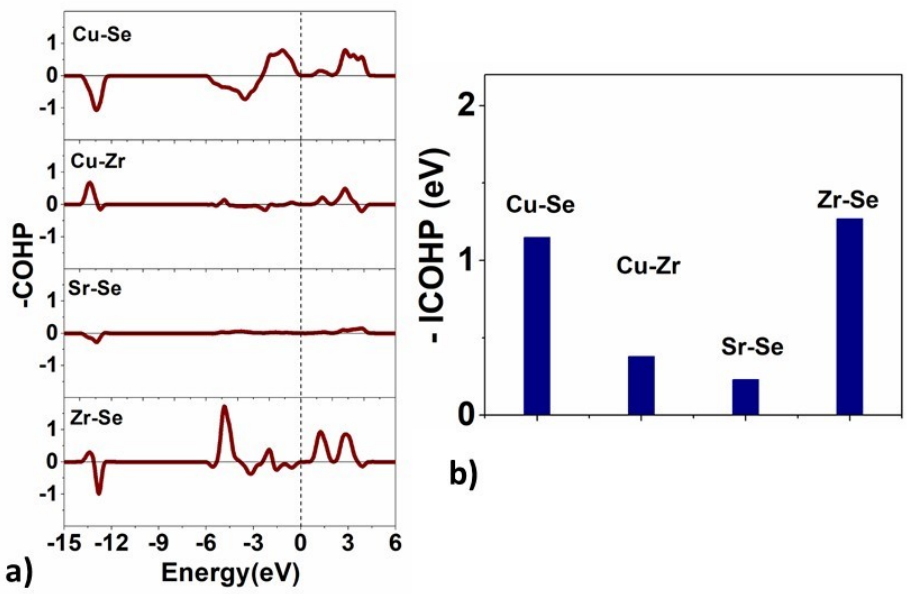

Fig. S5: (a) The crystal orbital Hamilton population (COHP) for the bonding pairs and the **(b)** integrated COHP values for the bonding pairs of the $Sr_3Zr_2Cu_4Se_9$ structure.

Section S4: A brief description of the GGA-1/2 exchange-correlation (XC) functional

The standard XC functionals, such as LDA and GGA, usually predict ground-state properties with good accuracy. However, the electronic properties, such as band gaps estimated by these functionals, are significantly smaller than the experimental values. These discrepancies are attributed to the self-interaction error and/or the lack of discontinuity of the XC potential in going from the valence to the conduction band. In the past, the Slater half-occupation technique and its formalization through the Janak theorem have been used, in particular for atoms, molecules, and clusters, for obtaining valence states with good accuracy comparable to the experimental ionization energies. The Janak theorem refers to the derivative of the total energy with respect to the occupation, which equals the Kohn-Sham (KS) eigenvalue. The half-occupation technique is generalized to extended systems such as crystals in the DFT-1/2 or GGA-1/2 technique, leading to good improvement in the band gap estimates. The GGA-1/2 technique also leads to partial self-interaction correction (SIC), which is missing in LDA or GGA techniques. The self-interaction correction (SIC) is defined as the difference between ionization energy (IE) and KS eigenvalue. It can be shown that the difference between the ionization energies (IE) and the KS eigenvalue is about 1/2 the SIC whenever the Janak theorem is valid, *i.e.*, when the energy functional can be differentiated with respect to the occupations.

Table S1 Fractional atomic coordinates and isotropic or equivalent isotropic displacement parameters (Å^2) for $Sr_3Zr_2Cu_4S_9$ structure.

Atoms	Wyckoff position	Site	*x*	*y*	*z*	U_{iso}/U_{eq}[a]
Sr(1)	2*i*	1	0.02289(12)	0.28554(8)	0.51275(8)	0.01222(15)
Sr(2)	2*i*	1	0.31226(11)	0.24359(8)	0.83113(7)	0.01079(15)
Sr(3)	2*i*	1	0.65550(12)	0.22878(8)	0.15896(8)	0.01431(16)
Zr(1)	2*i*	1	0.15760(11)	0.48816(7)	0.16002(7)	0.00766(14)
Zr(2)	2*i*	1	0.33865(11)	0.01423(7)	0.34348(7)	0.00718(14)
Cu(1)	2*i*	1	0.13492(19)	0.06372(14)	0.12061(12)	0.0228(3)
Cu(2)	2*i*	1	0.14085(16)	0.75657(10)	0.08159(11)	0.0141(2)
Cu(3)	2*i*	1	0.38946(18)	0.42707(14)	0.37034(12)	0.0232(3)
Cu(4)	2*i*	1	0.54004(16)	0.25993(11)	0.59811(11)	0.0149(2)
S(1)	2*i*	1	0.0449(3)	0.4329(2)	0.32921(18)	0.0086(3)
S(2)	2*i*	1	0.1314(3)	0.74945(18)	0.2769(2)	0.0075(3)
S(3)	2*i*	1	0.1810(3)	0.23431(19)	0.0458(2)	0.0102(3)
S(4)	2*i*	1	0.3007(3)	0.05853(18)	0.56325(19)	0.0085(3)
S(5)	2*i*	1	0.4108(3)	0.94792(19)	0.12704(17)	0.0082(3)
S(6)	2*i*	1	0.5537(3)	0.5469(2)	0.27355(18)	0.0096(4)
S(7)	2*i*	1	0.5563(3)	0.2616(2)	0.4062(2)	0.0105(3)
S(8)	2*i*	1	0.7594(3)	0.44509(18)	0.02277(19)	0.0080(3)
S(9)	2*i*	1	0.9856(3)	0.0653(2)	0.26874(18)	0.0094(3)

[a] U_{iso}/U_{eq} is the one-third trace value of the orthogonalized U_{ij} tensor.

Table S2 Fractional atomic coordinates and isotropic or equivalent isotropic displacement parameters (Å^2) for $Sr_3Zr_2Cu_4Se_9$ structure.

Atoms	Wyckoff position	Site	*x*	*y*	*z*	U_{iso}/U_{eq}[a]

Sr(1)	2*i*	1	0.0177(2)	0.27479(12)	0.51116(12)	0.0174(2)
Sr(2)	2*i*	1	0.31795(18)	0.25042(11)	0.83624(12)	0.0152(2)
Sr(3)	2*i*	1	0.65367(18)	0.23153(12)	0.15746(12)	0.0167(2)
Zr(1)	2*i*	1	0.16735(17)	0.48749(11)	0.16345(10)	0.0121(2)
Zr(2)	2*i*	1	0.34375(17)	0.01636(10)	0.33885(11)	0.0109(2)
Cu(1)	2*i*	0.598(8)	0.0897(5)	0.0033(4)	0.0892(3)	0.0359(11)
Cu(2)	2*i*	1	0.1397(3)	0.75482(16)	0.0801(2)	0.0232(4)
Cu(3)	2*i*	0.856(7)	0.2026(3)	0.24998(17)	0.2635(2)	0.0180(6)
Cu(4)	2*i*	0.532(8)	0.4123(6)	0.4937(4)	0.4138(4)	0.0331(12)
Cu(5)	2*i*	1	0.5365(3)	0.25604(15)	0.59738(18)	0.0184(3)
Se(1)	2*i*	1	0.04509(19)	0.43898(11)	0.33654(11)	0.0113(3)
Se(2)	2*i*	1	0.13032(17)	0.75022(10)	0.27656(12)	0.0096(2)
Se(3)	2*i*	1	0.18345(19)	0.22670(11)	0.05191(12)	0.0123(2)
Se(4)	2*i*	1	029579(17)	0.05392(11)	0.56151(11)	0.0107(2)
Se(5)	2*i*	1	0.41581(19)	0.94635(11)	0.12416(11)	0.0121(3)
Se(6)	2*i*	1	0.54698(18)	0.27205(12)	0.40371(12)	0.0124(2)
Se(7)	2*i*	1	0.56281(18)	0.54850(12)	0.27712(11)	0.0124(3)
Se(8)	2*i*	1	0.76031(17)	0.44678(11)	0.02464(11)	0.0107(2)
Se(9)	2*i*	1	0.97614(18)	0.05929(12)	0.26244(11)	0.0120(3)

[a] U_{iso}/U_{eq} is the one-third trace value of the orthogonalized U_{ij} tensor.

Table S3 Selected bond distances (Å) in the $Sr_3Zr_2Cu_4S_9$.

Atom pair	**Distances (Å)**	**Atom pair**	**Distances (Å)**
Zr(1)−S(1)	2.529(2)	Cu(4)−S(6)^{iv}	2.334(2)
Zr(1)−S(2)	2.638(2)	Cu(4)−S(7)	2.325(2)
Zr(1)−S(3)	2.560(2)	Sr(1)−S(1)^{ii}	3.046(2)
Zr(1)−S(6)	2.549(2)	Sr(1)−S(1)	3.075(2)

Zr(1)−S(8)^{viii}	2.656(2)	Sr(1)−S(2)^{ii}	3.051(2)
Zr(1)−S(8)^{i}	2.650(2)	Sr(1)−S(4)^{iii}	3.628(2)
Zr(2)−S(2)^{ix}	2.668(2)	Sr(1)−S(4)	3.270(2)
Zr(2)−S(4)	2.590(2)	Sr(1)−S(6)^{iv}	3.130(3)
Zr(2)−S(4)^{vi}	2.694(2)	Sr(1)−S(7)^{i}	3.007(2)
Zr(2)−S(5)^{ix}	2.625(2)	Sr(1)−S(9)^{i}	2.694(2)
Zr(2)−S(7)	2.549(2)	Sr(2)−S(2)^{ii}	2.944(2)
Zr(2)−S(9)^{i}	2.490(2)	Sr(2)−S(3)^{v}	2.935(2)
Cu(1)−S(3)	2.246(2)	Sr(2)−S(4)	3.103(2)
Cu(1)−S(5)^{ix}	2.312(2)	Sr(2)−S(5)^{iv}	2.938(2)
Cu(1)−S(9)^{i}	2.234(2)	Sr(2)−S(6)^{iv}	2.990(2)
Cu(2)−S(2)	2.372(2)	Sr(2)−S(8)^{v}	3.230 (3)
Cu(2)−S(3)^{x}	2.336(3)	Sr(2)−S(8)^{iv}	3.259(2)
Cu(2)−S(5)	2.326(2)	Sr(2)−S(9)^{vi}	3.213(3)
Cu(2)−S(8)^{viii}	2.309(2)	Sr(3)−S(1)^{viii}	2.924(3)
Cu(1)···Cu(1)^{xi}	2.753(3)	Sr(3)−S(3)	3.138(2)
Cu(1)···Cu(2)^{ix}	3.0504(18)	Sr(3)−S(5)^{ix}	3.009(2)
Cu(3)···Cu(3)^{iv}	2.845(3)	Sr(3)−S(5)^{viii}	3.172(2)
Cu(3)−S(1)	2.246(2)	Sr(3)−S(6)	3.330(2)
Cu(3)−S(6)	2.310(2)	Sr(3)−S(7)	3.102(2)
Cu(3)−S(7)	2.243(2)	Sr(3)−S(8)	3.274(2)
Cu(4)−S(2)^{iv}	2.359(3)	Sr(3)−S(9)	3.214(2)
Cu(4)−S(4)	2.315(2)		

Symmetry codes: (i) $x-1, y, z$; (ii) $-x, -y+1, -z+1$; (iii) $-x, -y, -z+1$; (iv) $-x+1, -y+1, -z+1$; (v) $x, y, z+1$; (vi) $-x+1, -y, -z+1$; (vii) $x+1, y, z$; (viii) $-x+1, -y+1, -z$; (ix) $x, y-1, z$; (x) $-x, -y+1, -z$; (xi) $-x, -y, -z$; (xii) $x, y+1, z$; (xiii) $x, y, z-1$.

Table S4 Selected bond distances (Å) in the $Sr_3Zr_2Cu_4Se_9$.

Atom pair	**Distances (Å)**	**Atom pair**	**Distances (Å)**
Zr(1)−Se(1)	2.6681(18)	Cu(4)−Se(1)	2.411(4)
Zr(1)−Se(2)	2.7701(17)	Cu(4)−Se(6)	2.623(4)
Zr(1)−Se(3)	2.7021(17)	Cu(4)−Se(6)^{iv}	2.682(5)
Zr(1)−Se(7)	2.6342(19)	Cu(4)−Se(7)	2.390(4)

Zr(1)−Se(8)^{i}	2.7982(19)	Cu(5)−Se(2)^{iv}	2.451(2)
Zr(1)−Se(8)^{vii}	2.7765(18)	Cu(5)−Se(4)	2.415(2)
Zr(2)−Se(2)^{ix}	2.8083(18)	Cu(5)−Se(6)	2.463(2)
Zr(2)−Se(4)	2.7515(18)	Cu(5)−Se(7)^{iv}	2.450(2)
Zr(2)−Se(4)^{vi}	2.7919(18)	Sr(1)−Se(1)^{ii}	3.1674(19)
Zr(2)−Se(5)^{ix}	2.6981(18)	Sr(1)−Se(2)^{ii}	3.1281(19)
Zr(2)−Se(6)	2.6821(18)	Sr(1)−Se(4)	3.3299(19)
Zr(2)−Se(9)^{i}	2.6358(17)	Sr(1)−Se(4)^{iii}	3.614(2)
Cu(1)−Se(3)	2.619(4)	Sr(1)−Se(6)^{i}	3.192(2)
Cu(1)−Se(3)^{xi}	2.657(5)	Sr(1)−Se(7)^{iv}	3.222(2)
Cu(1)−Se(5)^{ix}	2.388(4)	Sr(1)−Se(9)^{i}	3.081(2)
Cu(1)−Se(9)^{i}	2.386(4)	Sr(2)−Se(2)^{ii}	3.0654(19)
Cu(2)−Se(2)	2.451(3)	Sr(2)−Se(3)^{v}	3.1134(19)
Cu(2)−Se(3)^{x}	2.476(3)	Sr(2)−Se(4)	3.293(2)
Cu(2)−Se(5)	2.452(2)	Sr(2)−Se(5)^{iv}	3.0322(18)
Cu(2)−Se(8)^{vii}	2.405(2)	Sr(2)−Se(7)^{iv}	3.0707(19)
Cu(1)···Cu(1)^{xi}	2.193(6)	Sr(2)−Se(8)^{iv}	3.3100(19)
Cu(1)···Cu(2)^{ix}	2.687(4)	Sr(2)−Se(9)^{vi}	3.335(2)
Cu(1)···Cu(3)	2.661(5)	Sr(3)−Se(1)^{viii}	3.073(2)
Cu(3)···Cu(4)	2.621(5)	Sr(3)−Se(3)	3.180(2)
Cu(4)···Cu(4)^{iv}	2.101(7)	Sr(3)−Se(5)^{ix}	3.142(2)
Cu(4)···Cu(5)^{iv}	2.711(4)	Sr(3)−Se(6)	3.214(19)
Cu(3)−Se(1)	2.436(2)	Sr(3)−Se(7)	3.4277(19)
Cu(3)−Se(3)	2.498(3)	Sr(3)−Se(8)	3.3520(19)
Cu(3)−Se(6)	2.492(3)	Sr(3)−Se(9)	3.329(2)
Cu(3)−Se(9)	2.426(2)		

Symmetry codes: (i) $x-1, y, z$; (ii) $-x, -y+1, -z+1$; (iii) $-x, -y, -z+1$; (iv) $-x+1, -y+1, -z+1$; (v) $x, y, z+1$; (vi) $-x+1, -y, -z+1$; (vii) $-x+1, -y+1, -z$; (viii) $x+1, y, z$; (ix) $x, y-1, z$; (x) $-x, -y+1, -z$; (xi) $-x, -y, -z$; (xii) $x, y, z-1$; (xiii) $x, y+1, z$.

References

1K. Srivastava, O. Shahid, A. K. Ray, M. Deepa, M. K. Niranjan and J. Prakash, *J. Phys.*

Chem. Solids, 2024, **192**, 112085.

2 A. Yadav, P. Deshmukh, K. Roberts, N. Jisrawi and S. Valluri, *J. Phys. Commun.*, 2019, **3**, 105001.

3 W. Kohn and L. J. Sham, *Phys. Rev.*, 1965, **140**, A1133–A1138.

4 P. E. Blöchl, *Phys. Rev. B*, 1994, **50**, 17953–17979.

5 J. P. Perdew, K. Burke and M. Ernzerhof, *Phys. Rev. Lett.*, 1996, **77**, 3865–3868.

6 L. G. Ferreira, M. Marques and L. K. Teles, *Phys. Rev. B*, 2008, **78**, 125116.

7 G. Kresse and J. Furthmüller, *Phys. Rev. B*, 1996, **54**, 11169–11186.